


Electromagnetically induced transparency in many-emitter waveguide quantum electrodynamics: Linear versus nonlinear waveguide dispersions

Tiberius Berndsen and Imran M. Mirza^{✉*}*Macklin Quantum Information Sciences, Department of Physics, Miami University, Oxford, Ohio 45056, USA*
 (Received 7 July 2023; revised 11 November 2023; accepted 20 November 2023; published 4 December 2023)

We study single-photon-induced electromagnetically induced transparency (EIT) in many-emitter waveguide quantum electrodynamics (wQED) with linear, nonlinear, and quasilinear waveguide dispersion relations. In the single-emitter problem, in addition to the robustness of the EIT spectral features in the overcoupled regime of wQED, we find that the nonlinear dispersion results in the appearance of a side peak for frequencies smaller than the resonant EIT frequency, which turns into a plateau as the nonlinearity is reduced. The quasilinear case produces a similar spectrum to the purely linear scenario with a small observable difference in the far-detuned regime. Consequently, for many-emitter scenarios, our results indicate the formation of band structure for purely linear cases, which, for smaller values of nonlinearity, leads to a narrow band-gap-like structure compared to the corresponding linear and quasilinear dispersion cases. Long-distance quantum networking aided with quantum memories can serve as one of the targeted applications of this work.

DOI: [10.1103/PhysRevA.108.063702](https://doi.org/10.1103/PhysRevA.108.063702)

I. INTRODUCTION

Electromagnetically induced transparency or EIT is a coherent optical phenomenon where, under the right conditions of resonant transitions and atomic decay rates, a weak probe light beam, in the presence of a strong pump field, can pass through a three-level atomic medium with 100% transmission rate [1,2]. In addition to providing this remarkable transparency feature, EIT also allows the manipulation of dispersion properties of the probe field, leading to fascinating effects such as slow, stopped, and fast light [3–5]. These two features combined, EIT in the last two decades has witnessed a range of applications from quantum information storage [6,7] to magnetometry [8] to the development of more precise atomic clocks [9].

In this work, we study EIT in waveguide quantum electrodynamics or wQED: quantum emitters (natural or artificial atoms, quantum dots, or qubits) coupled to optical fields guided by one-dimensional (1D) bosonic fibers or waveguides [10–12]. In its simplest setting, a wQED setup consists of a single two-level quantum emitter coupled with a bidirectional waveguide with linear dispersive properties [13]. However, for EIT's observation, one must utilize a three-level quantum emitter in which two atomic transitions, initiated from two different energy levels, are guided to a common final state [14].

To date, the literature on the topic of EIT in wQED has remained limited to either the case in which a chain of three-level atoms coupled to a waveguide with linear dispersion [14–16] or to a single three-level atom coupled to a nonlinear waveguide [17,18]. Relevant to this are also the studies in which single or many but two-level quantum emitters interact with a nonlinear dispersive waveguide [19–23] or strong

interaction at the few-photon level has been established in a waveguide with a nonlinear medium [24,25]. However, none of the previous works studied EIT in the case of an array of three-level emitters coupled to a 1D waveguide with nonlinear and quasilinear dispersion relations. In this paper, we address this problem, keeping in view the rich many-body physics of a one-dimensional periodic lattice of quantum emitters coupled to guided photonic modes [26–28].

As for some key results, we find that, for single-emitter problems, the nonlinear dispersion relation can result in an additional side peak at smaller frequencies (compared to the EIT peak frequency), which forms the shape of a transmission plateau for weaker nonlinear dispersion relations. The quasilinear case shows spectral features similar to the purely linear case for the single quantum emitter problem. For many-emitter lattices, we utilized the transfer matrices framework [29,30]. Therein, we observe that due to quantum interference, the photon transmission properties exhibit band structure for linear dispersion whose gap tends to elevate with reduced nonlinear dispersion. The quasilinear dispersion exhibited band gap behavior more similar to the nonlinear case. Our results indicate that the nonlinear and quasilinear dispersion of the waveguide allows novel ways of controlling the single-photon propagation in three-level wQED chains with potential applications in long-distance quantum networking and communications [31].

The paper is structured as follows. In Sec. II, we begin by recapping the problem of single-photon transport through a three-level wQED setup with linear dispersion [14,32]. Next, in Sec. III, we examine the same problem for nonlinear dispersive waveguides. We devote Sec. IV to discussing quasilinear dispersion (where both linear and quadratic nonlinear dispersion can coexist) and in Sec. V we discuss the novel problem of periodic chains of three-level quantum emitters while comparing the transmission spectra and dispersion curves for the

*mirzaim@miamioh.edu

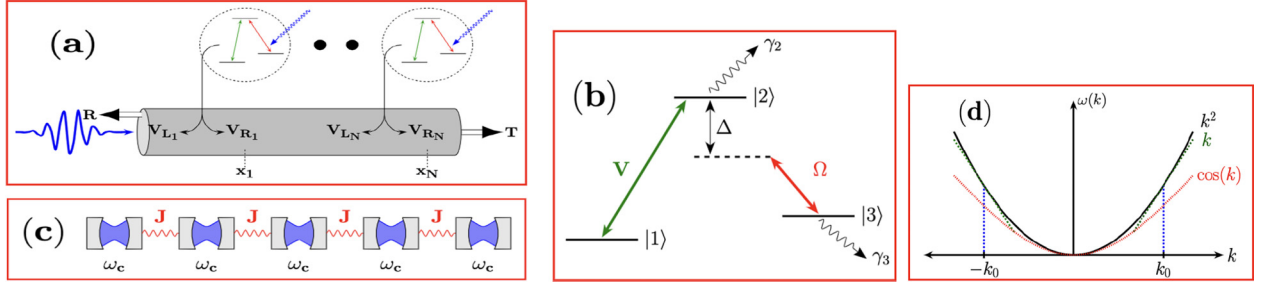


FIG. 1. (a) Setup: A bidirectional waveguide with linear, nonlinear, or quasilinear dispersion is side coupled to a chain of three-level quantum emitters, with left (right) emitter-waveguide coupling strength V_{L_j} (V_{R_j}) for the j th quantum emitter ($1 \leq j \leq N$). For simplicity, throughout this work, we will assume a symmetric coupling case in which $V_{L_j} = V_{R_j} = V$. Each quantum emitter is excited by a pump field and an incoming single photon. (b) Energy-level diagram of the three-level quantum emitter: Emitter-waveguide coupling drives the transition $|1\rangle \longleftrightarrow |2\rangle$ with coupling strength V while the transition $|2\rangle \longleftrightarrow |3\rangle$ is driven by a strong pump field with Rabi frequency Ω and detuning Δ . Δ has been exaggerated for visual clarity. The decay rates are γ_2 and γ_3 from the states $|2\rangle$ and $|3\rangle$, respectively. (c) Nonlinear waveguide model: Waveguide here consists of a 1D array of coupled resonators with an identical frequency ω_c and a photon hopping rate J between two consecutive resonators. Under the tight-binding approximation, such a setup is known to offer a cosine-like nonlinear dispersion. (d) Approximations of the nonlinear dispersion: Quadratic and linear approximations of a cosine dispersion relation are shown. For simplicity, the lattice constant has been set equal to unity.

linear, nonlinear, and quasilinear cases. Finally, we close with the main conclusions in Sec. VI.

II. LINEAR DISPERSION CASE: SINGLE QUANTUM EMITTER PROBLEM

As shown in Fig. 1(a), the Hamiltonian for the system under study can be decomposed into three pieces

$$\hat{H} = \hat{H}_W + \hat{H}_{QE} + \hat{H}_I, \quad (1)$$

where \hat{H}_W , \hat{H}_{QE} , and \hat{H}_I represent the free waveguide, free three-level quantum emitter, and interaction Hamiltonian, respectively. We first focus on our three-level Λ -type quantum emitter Hamiltonian [33]. As mentioned in Fig. 1(b), the quantum emitter Hamiltonian \hat{H}_{QE} can be expressed as (with $\hbar = 1$)

$$\hat{H}_{QE} = \tilde{\omega}_2 |2\rangle\langle 2| + \tilde{\omega}_3 |3\rangle\langle 3| + \frac{\Omega}{2} (|3\rangle\langle 2| + \text{H.c.}), \quad (2)$$

where we adopt a short notation in which $\tilde{\omega}_2 \equiv \omega_2 - \frac{i\gamma_2}{2}$, $\tilde{\omega}_3 \equiv \omega_2 - \Delta - \frac{i\gamma_3}{2}$, and H.c. abbreviates the Hermitian conjugate of the first term in the parentheses. In the real-space formalism of quantum optics [34,35], the waveguide Hamiltonian in the linear dispersion regime takes the following form:

$$\hat{H}_W^{(L)} = iv_g \int (\hat{c}_L^\dagger \partial_x \hat{c}_L - \hat{c}_R^\dagger \partial_x \hat{c}_R) dx, \quad (3)$$

with v_g being the group velocity of the photon in the waveguide. Finally, under the rotating wave approximation, we write the interaction Hamiltonian in the following fashion:

$$\hat{H}_I = \sum_{d=L,R} \int \delta(x) V (\hat{c}_d^\dagger(x) |1\rangle\langle 2| + \text{H.c.}) dx. \quad (4)$$

Here $d = L$ (R) represents left (right) propagating photons in the waveguide and \hat{c}_d represents annihilation operators for the d th direction. The real-valued parameter V quantifies the emitter-waveguide interaction strength for the transition $|1\rangle \longleftrightarrow |2\rangle$ with the Dirac delta function specifying the

location of the quantum emitter. Next, in the single excitation sector of the Hilbert space, we write the quantum state of the system as

$$|\Psi\rangle = \left[\sum_{d=L,R} \int \varphi_d(x) \hat{c}_d^\dagger dx + \sum_{j=2,3} e_j |j\rangle \langle 1| \right] |\emptyset\rangle, \quad (5)$$

where $|\emptyset\rangle$ represents the ground state of the system (i.e., quantum emitter being unexcited and no photons in the waveguide). By inserting Eqs. (1) and (5) into the time-independent Schrödinger equation $\hat{H}|\Psi\rangle = \hbar\omega|\Psi\rangle$ we arrive at the following coupled equations for the amplitudes:

$$-iv_g \varphi_R(x) + Ve_2 \delta(x) = \omega \varphi_R(x), \quad (6a)$$

$$iv_g \varphi_L(x) + Ve_2 \delta(x) = \omega \varphi_L(x), \quad (6b)$$

$$V_R \varphi_R(0) + V \varphi_L(0) + \frac{\Omega}{2} e_3 = (\omega - \tilde{\omega}_2) e_2, \quad (6c)$$

$$\frac{\Omega}{2} e_2 = (\omega - \tilde{\omega}_3) e_3, \quad (6d)$$

where $\hbar\omega$ is the energy of the photon incident from the left end of the waveguide. Our aim now is to calculate the single-photon transmission and reflection probabilities, and for that we assume the left and right field amplitudes obey the following ansatzes:

$$\varphi_R(x) = e^{ikx} \Theta(-x) + t e^{ikx} \Theta(x), \quad (7a)$$

$$\varphi_L(x) = r e^{-ikx} \Theta(-x). \quad (7b)$$

Here t and r are the transmission and reflection coefficients related to the transmission and reflection probabilities through $|t|^2 = T$ and $|r|^2 = R$. With this the amplitude equations for $\varphi_{R/L}(x)$ becomes

$$iv_g(1-t) + Ve_2 = 0, \quad (8a)$$

$$-iv_g r + Ve_2 = 0, \quad (8b)$$

$$\frac{V}{2}(t+1) + \frac{V}{2}r + \frac{\Omega}{2}e_3 = (\omega - \tilde{\omega}_2)e_2. \quad (8c)$$

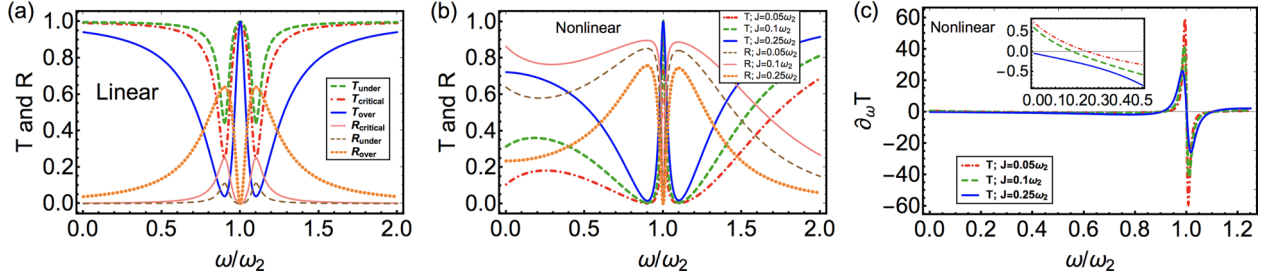


FIG. 2. Single-photon T and R probability as a function of frequency ω for the single quantum emitter ($N = 1$) problem in the (a) linear dispersion case with critical coupling regime $\Gamma = \gamma_2$, undercoupled regime $\Gamma = \gamma_2/2$, and overcoupled regime $\Gamma = 4\gamma_2$. (b) Nonlinear case. In all curves, we selected an overcoupled regime, which, for the nonlinear case, means $V = \sqrt{0.2}\omega_2$ and varied values of J . (c) The derivative of T with respect to photon frequency ω is used to examine the dependence of transmission around $\omega = \omega_2/4$ region in the nonlinear case on different values of J . The inset plot curves show the magnified version of $\partial_\omega T$ in the region $0 \leq \omega \leq \omega_2/2$ again for different J values. The common parameters used in all plots are $\Omega = 0.2\omega_2$, $\gamma_2 = 0.1\omega_2$, $\gamma_3 = 0$, and $\Delta = 0$.

The solution of this set of coupled equations yields the transmission and reflection amplitudes for the linear (l) waveguide dispersion case as given by

$$t^{(l)} = \frac{(\omega - \tilde{\omega}_3)(\omega - \tilde{\omega}_2) - \Omega^2/4}{(\omega - \tilde{\omega}_3)[(\omega - \tilde{\omega}_2) + i\Gamma/2] - \Omega^2/4}, \quad (9)$$

$$r^{(l)} = \frac{-i\Gamma/2(\omega - \tilde{\omega}_3)}{(\omega - \tilde{\omega}_3)[(\omega - \tilde{\omega}_2) + i\Gamma/2] - \Omega^2/4}, \quad (10)$$

with $\Gamma \equiv \frac{2V^2}{v_g}$ being the emitter-waveguide coupling rate.

From this point onward, we will work in a unit system where, for the sake of simplicity, the speed of light (either group or phase velocity) has been set equal to 1. We point out that these results were already reported for the single three-level quantum emitter problem by Witthaut *et al.* and Mirza *et al.* [14,17,32].

In Fig. 2(a) we plot the $T(\omega)$ and $R(\omega)$ for the linear dispersion case. By selecting the experimentally feasible parameters inspired from Ref. [32] we consider three cases based on how emitter-waveguide coupling rate Γ compares with the decay rate γ_2 . We find that, in the overcoupled case (solid blue curve), T exhibits closest to the perfect EIT pattern where the maximum transmission occurs at $\omega = \omega_2$ and the linewidth of the transparency window is controlled by the Rabi frequency Ω . The emitter-waveguide coupling parameter Γ can also manipulate the shallowness and width of the two side peaks occurring at $\omega = \pm\Omega/2$ under $\Delta = 0$ and $\gamma_3 = 0$ conditions. These side peaks originate from the reflection and, therefore, the interference of photons. Finally, we indicate that in the overcoupling regime, four points exist where T and R curves intersect, allowing the preparation of single-photon quantum superposition states of transmission and reflection (see, for instance, Refs. [13,28] for a similar behavior for the two-level quantum emitter wQED).

III. NONLINEAR DISPERSION CASE: SINGLE QUANTUM EMITTER PROBLEM

We now turn our attention to the corresponding nonlinear dispersion regime for the single quantum emitter case. To this end, we consider a waveguide model consisting of a one-dimensional array of coupled Fabry-Perot cavities [as shown in Fig. 1(c)]. Under the tight-binding approximation, such a

model is known to generate a cosine dispersion relation of the form $\omega(k) = \omega_J - 2J \cos(kL)$ [19,36] [see Fig. 1(d)], where ω_J represents the average ω_k value in the cosine curve. As derived in the Appendix, in comparison to the linear case, we describe the free waveguide Hamiltonian in Eq. (3) in the nonlinear (nl) case as

$$\hat{\mathcal{H}}_W^{(nl)} = -2J \sum_{d=L,R} \int \hat{c}_d^\dagger(x) \left(\sum_{j=0}^{\infty} \frac{\partial_x^{2j}}{(2j)!} \right) \hat{c}_d(x) dx, \quad (11)$$

where we set $\omega_J = 0$. As discussed by Zhou *et al.* [19] and others (see, for example, Ref. [23]), under the low-energy limit, i.e., when the wavelength $\lambda \gg L$, such a cosine dispersion is known to produce a quadratic dependence of the form $\omega(k) \sim Jk^2$ (here k is treated dimensionless). Whereas, at the so-called matching condition of $\lambda = 4L$, the same dispersion can also offer linear dispersion with $\omega(k) \sim -2Jk$. This section restricts our discussion to the low-energy regime, where the dispersion relation will be purely quadratic. A more general treatment of quasilinear dispersion [37] (where linear and quadratic terms coexist) is presented in Sec. IV. Thus, proceeding further, we truncate the cosine dispersion to the quadratic level [as shown in Fig. 1(d)]. Following the same calculations, we arrive at four coupled equations. Only Eqs. (6a) and (6b) change and take the new form as

$$-J\partial_x^2 \varphi_d(x) + Ve_2 \delta(x) = \omega \varphi_d(x). \quad (12)$$

We note that the prefactors of iv_g appearing in the linear case with opposite signs for the left and right directions [see Eqs. (6a) and (6b)] have now been swapped with the second-order derivative term times the hopping rate with the same negative sign for both $d = L$ and $d = R$. Next, we integrate the above equation over the interval $[0 - \epsilon, 0 + \epsilon]$ with ϵ being a small positive number. This yields the following jump condition on the derivative of $\varphi_d(x)$:

$$J \left[\partial_x \varphi_d(x) \Big|_{x=-\epsilon}^{x=+\epsilon} \right] = Ve_2, \quad \forall d = L, R.$$

Next, we use the ansatz mentioned in Eq. (7). We thus arrive at the following set of equations in terms of t and r as

$$-iJk(t-1) + Ve_2 = 0, \quad \text{and} \quad -iJkr + Ve_2 = 0. \quad (13)$$

Solving for the transmission and reflection coefficients in the nonlinear (nl) regime yields

$$t^{(nl)} = \frac{k[(\omega - \tilde{\omega}_2)(\omega - \tilde{\omega}_3) - \Omega^2/4]}{(\omega - \tilde{\omega}_3)[k(\omega - \tilde{\omega}_2) + iV^2/J] - k\Omega^2/4}, \quad (14a)$$

$$r^{(nl)} = \frac{iV^2(\omega - \tilde{\omega}_3)/J}{(\omega - \tilde{\omega}_3)[k(\omega - \tilde{\omega}_2) + iV^2/J] - k\Omega^2/4}, \quad (14b)$$

where for the nonlinear case $k = \sqrt{2 + \omega/J}$ [note that the positive momentum (or $\hbar k$) values are selected for the sake of simplicity]. In Fig. 2(b), we plot the transmission T and reflection R probability as a function of ω for the nonlinear problem under the overcoupling regime. We find that the overall T shape remains intact, indicating the robustness of EIT in the overcoupling regime. Second, as we decrease the nonlinearity (J value), a side peak emerges around the $\omega \sim \omega_2/4$ point. Interestingly, this peak forms an almost plateau shape as we approach the nonlinearity value of $J = 0.05\omega_2$. As shown in Fig. 2(c), the behavior of this plateau can be analyzed by considering the derivative $\partial_\omega T$ (a mathematical expression not reported here due to complexity). We find that, around $\omega = \omega_2/4$, this derivative function remains nonpositive for higher values of J (see, for example, the blue solid curve corresponding to $J = 0.25\omega_2$). However, as we begin to decrease the value of J and consider the cases of $J = 0.1\omega_2$ or $J = 0.05\omega_2$, the slope of $T(\omega)$ changes sign around $\omega = \omega_2/4$ which provides numerical evidence of the dependence of this additional peak formation on the J value. At this point, we would like to highlight that this low-frequency spectral feature is peculiar to the nonlinear case (with no counterpart in the linear case) and can be used to manipulate the photon transport properties in novel ways without disturbing the advantages of the EIT spectrum.

IV. QUASILINEAR DISPERSION REGIME

The presence of a purely quadratic dispersion considered in the previous section may only be present in the low-energy approximation of the special cosine dispersion encountered in a coupled cavity array model of the waveguide [19,23,36]. In a general situation (discussed in this section), a photon launched into a waveguide with momentum k_0 would experience a dispersion of the form

$$\omega(k) = \omega(k_0) + (k - k_0) \left. \frac{\partial \omega}{\partial k} \right|_{k=k_0} + \frac{1}{2!} (k - k_0)^2 \left. \frac{\partial^2 \omega}{\partial k^2} \right|_{k=k_0} + \dots \quad (15)$$

By calling $\left. \frac{\partial \omega}{\partial k} \right|_{k=k_0} = v_g$ and $\left. \frac{\partial^2 \omega}{\partial k^2} \right|_{k=k_0} = \xi$, in the following we work under the assumption $|\xi/v_g| < 1$ (with $L = 1$) which allows us to truncate the aforementioned Taylor expansion at the quadratic level. Furthermore, we set k_0 and $\omega(k_0)$ as the reference wave number or momentum and angular frequency. We thus arrive at the following quasilinear (ql) dispersion relation [37]:

$$\omega(k) \approx \eta v_g k + \frac{1}{2} \xi k^2, \quad (16)$$

where $\eta = \{-1, 1\}$ depending on the left and right directions in the waveguide. Such a dispersion relation produces the following modified bidirectional waveguide Hamiltonian as compared to the linear case

$$\hat{\mathcal{H}}_W^{(ql)} = \int \left(\hat{c}_L^\dagger(x) \left[i v_g \partial_x - \frac{1}{2} \xi \partial_x^2 \right] \hat{c}_L(x) - \hat{c}_R^\dagger(x) \left[i v_g \partial_x + \frac{1}{2} \xi \partial_x^2 \right] \hat{c}_R(x) \right) dx. \quad (17)$$

Following the same lines of calculations as before, we obtain the transmission and reflection coefficients for the quasilinear case as

$$t^{(ql)} = \frac{[(\omega - \tilde{\omega}_2)(\omega - \tilde{\omega}_3) - \Omega^2/4] \tilde{k}}{[(\omega - \tilde{\omega}_2)(\omega - \tilde{\omega}_3) - \Omega^2/4] \tilde{k} + 2iV^2(\omega - \tilde{\omega}_3)}, \quad (18a)$$

$$r^{(ql)} = \frac{-2iV^2(\omega - \tilde{\omega}_3)}{[(\omega - \tilde{\omega}_2)(\omega - \tilde{\omega}_3) - \Omega^2/4] \tilde{k} + 2iV^2(\omega - \tilde{\omega}_3)}, \quad (18b)$$

where $\tilde{k} \equiv (k\xi + 2v_g)$ which has the units of frequency (as k is dimensionless).

V. EXTENSION TO MANY-EMITTER CASE: PHOTONIC BANDS

We now extend our single quantum emitter setup to the scenario in which a periodic chain of identical three-level quantum emitters is coupled with bidirectional waveguide fields. For the single photon problem, it is well known that t and r coefficients between consecutive atoms can be adequately linked in terms of transfer matrices [30]. Such a transfer matrix consists of two parts, namely, a part representing the response of a quantum emitter (\mathbf{M}_{QE}) and a part showing the free propagation of the photon in the waveguide between two consecutive atoms (\mathbf{M}_F). Under time-reversal symmetry restrictions \mathbf{M}_{QE} and \mathbf{M}_F can be generically written as [19,30]

$$\mathbf{M}_{QE} = \begin{bmatrix} 1/t^* & -r^*/t^* \\ -r/t & 1/t \end{bmatrix}, \quad \text{and} \quad \mathbf{M}_F = \begin{bmatrix} e^{ikL} & 0 \\ 0 & e^{-ikL} \end{bmatrix}, \quad (19)$$

where t and r can be transmission and reflection coefficients for linear $k = \omega/v_g$ or nonlinear $k = \sqrt{2 + \omega/J}$ or $\tilde{k} \equiv (k\xi + 2v_g)$ for quasilinear problems. The free propagation introduces time delays in the problem necessary to distinguish between Markovian and non-Markovian regimes of wQED [38]. Moving forward, we concentrate on the Markovian regime and divide the many quantum emitter problem into N segments or blocks where each block consists of a single quantum emitter and a free propagating region leading to the form of the transfer matrix of a single block as $\mathbf{M}_B = \mathbf{M}_{QE} \times \mathbf{M}_F$.

For a chain of identical quantum emitters, by applying Chebyshev's identity [39], we can arrive at an expression for the net transmission T_N for the resonant mode q under the

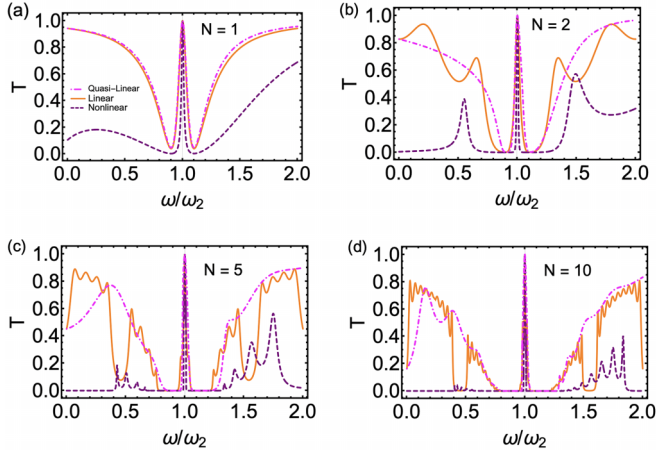


FIG. 3. Single-photon transport properties for a periodic chain consisting of (a) one, (b) two, (c) five, and (d) ten identical quantum emitters coupled with the bidirectional waveguide. Linear (solid orange curve), nonlinear or quadratic (dashed purple curve), and quasilinear regime (dotted-dashed magenta curve) are plotted for comparison in each plot. In all plots, we select an overcoupling regime with $\Gamma = 4\gamma_2$ in the linear case, a weak nonlinearity of $J = 0.05\omega_2$ in the nonlinear case, and $\xi = v_g/4$ for the quasilinear case. Both in nonlinear and quasilinear cases, $V = \sqrt{0.2}\omega_2$ is selected. The lattice constant L is set equal to unity. The rest of the parameters are the same as in Fig. 2.

no-loss scenario as

$$T_N = \left(1 + \frac{|r^2| \sin^2(NqL)}{|t^2| \sin^2(qL)} \right)^{-1}. \quad (20)$$

In Fig. 3, we plot the net $T_N(\omega)$ for a chain of up to $N = 10$ quantum emitters coupled with a waveguide with linear, nonlinear dispersion, and quasilinear dispersion. In all plots, we observe the robustness of EIT in the overcoupling regime. For the single quantum emitter problem, we observe that the quasilinear dispersion produces a transmission behavior very similar to the linear case with the slight departure of the trend observed in the detuned regime [for instance, around $\omega = 1.5\omega_2$ point in Fig. 3(a)].

For a large number of quantum emitters, we find the formation of photonic bands most visible in the linear dispersion case. In the multiemitter nonlinear case, we observe the emergence of a pattern consisting of consecutive peaks, which seems to indicate the partial formation of bands due to interference. The difference between the purely linear and nonlinear dispersion cases is most pronounced around $\omega \sim 0.25\omega_2$ and $1.25\omega_2 \leq \omega \leq 2\omega_2$ regions for the $N = 10$ emitter chain. It is known that such bands are formed due to interference between transmitted and reflected amplitudes from each quantum emitter boundary, which for a large quantum emitter number reduces to a sharper frequency combs pattern with applications in atomic clocks, spectroscopy, and metrology [40]. As the number of quantum emitters increases, the quasilinear case begins to exhibit spectral features disparate from the purely linear or purely nonlinear or quadratic case. For example, similar to the linear case, $T^{(ql)}$ takes higher values as we move away from the resonance ($\omega = \omega_2$). Still,

unlike the linear case, besides a null transmission region around the EIT peak, $T^{(ql)}$ fails to form distinct band gaps for detuned frequencies.

Next, to examine the photon's dispersion characteristics, we consider an infinitely long quantum emitter chain with lattice constant L . Applying the Bloch theorem [41] with K being the Bloch vector we obtain

$$\cos(KL) = \frac{1}{2} \text{tr}\{\mathbf{M}_B\} = \text{Re} \left[\frac{e^{-ikL}}{t} \right]. \quad (21)$$

Inserting the transmission coefficients $t^{(l)}$ and $t^{(nl)}$ in the last equation, we arrive at the following dispersion relations for linear and nonlinear cases as

$$(l) : \cos(KL) = \cos(kL) + \sin(kL) \left\{ \frac{\Gamma \delta_3}{2\Lambda^2} \right\}, \quad (22a)$$

$$(nl) : \cos(KL) = \cos(kL) + \sin(kL) \left\{ \frac{V^2 \delta_3}{\Lambda^2 k J} \right\}, \quad (22b)$$

where $\Lambda^2 = \delta_2 \delta_3 - \Omega^2/4$ with $\delta_j = \omega - \omega_j$, $\forall j = 2, 3$. The expression of the dispersion relation for the quasilinear case turns out to be mathematically involved and thus not reported here. In Fig. 4, we plot the dispersion curves for the linear, nonlinear, and quasilinear cases. For simplicity, we select $\gamma_2 = \gamma_3 = 0$ in all plots and $J = 0.05\omega_2$ for the nonlinear case. Furthermore, we chose L to be much smaller than the characteristic wavelength λ_0 (corresponding to the transition $|1\rangle \longleftrightarrow |2\rangle$) to make the forbidden bands more visible. As one of the main results, we observe that nonlinearity can be used to drastically control the forbidden bands' width. For instance, a weak nonlinearity of $J = 0.05\omega_2$ can increase the width of the forbidden band (green shaded region) by a factor of ~ 3 compared to the corresponding linear case.

The difference in the width of the photonic band gap introduced by the nonlinearity can be quantified through the function $\Delta\omega_B^{(nl)}$, where $\Delta\omega_B^{(nl)}$ is the difference between the ω value at which the band gap ends and $\omega/\omega_2 = 1.064$. Through numerical evidence, we find that the following linear relationship can approximate such a band gap, $\Delta\omega_B^{(nl)}(J)/\omega_2 \approx mJ + b$ [see inset of Fig. 4(b)]. For the case of $L = 0.045\lambda_0$, the slope $m = -0.552$ and the intercept $b = 2.396$ suffice. This approximate behavior shows that the difference in the band gap grows as one decreases J , again indicating the control on the band structure provided by the weak nonlinearity.

Finally, in Fig. 4(c), we plot the dispersion curve for the quasilinear case. Interestingly, we note a resemblance in the band-gap structure between purely nonlinear and quasilinear cases [compare Fig. 4(b) with Fig. 4(c)], which includes more significant band gaps and the absence of a higher ω -value dispersion branch for $L = 0.0112\lambda_0$ case [see Fig. 4(a) where this branch originates at $\omega = 3\omega_2$ in the linear case]. The behavior suggests that, with a periodic chain with infinitely many emitters (as considered in plotting dispersion curves), the nonlinear contribution in the quasilinear case begins to match the purely weakly nonlinear case.

VI. SUMMARY AND CONCLUSION

In this work, we examined the single-photon transport properties in three-level quantum emitter chains coupled with

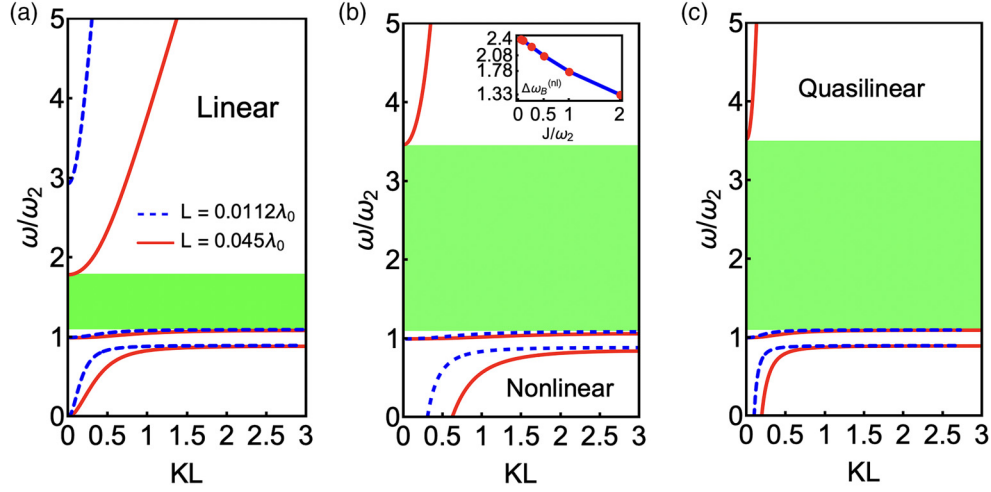


FIG. 4. Dispersion curves for a (a) linear, (b) nonlinear, and (c) quasilinear waveguide QED setup. In each plot, two closely spaced interatomic separations are selected. The inset in (b) indicates the difference between band gap $\Delta\omega_B$ for linear and nonlinear cases plotted against the nonlinearity parameter J (red dots are points indicating the difference in the width of the band gaps at specific J values while the blue curve is a linear fit as discussed in the text). The rest of the parameters are as used in Fig. 2.

1D waveguides with linear, nonlinear, and quasilinear dispersions. In the single-emitter case, we found that linearly dispersive waveguides lead to the standard EIT spectrum in the overcoupling regime. In the nonlinear case, at the quadratic level, we found that the EIT profile prevails as we decrease the strength of the nonlinearity parameter of dispersion. However, for smaller frequencies, we observed the formation of a plateau-like shape in the transmission spectrum. The quasilinear case showed transmission, which was quite similar to the linear case.

In the many-emitter overcoupling case, we noticed the formation of band structures where EIT spectral features remain intact. Again, the difference between the linear and nonlinear dispersions was most pronounced for smaller nonlinearity. Finally, the photonic band gaps were investigated using the Bloch theorem, where we mainly found the broadening of band gaps for decreased values of nonlinearity for smaller interemitter separations. The same trend of more significant band gaps was observed for the quasilinear dispersions. Our results revealed that nonlinear or quadratic and quasilinear wQED provide new ways of controlling the transport properties of single photons with possible applications in quantum memory-enabled long-distance quantum communication protocols.

ACKNOWLEDGMENTS

This work is supported by the NSF Grant No. LEAPS-MPS 2212860 and the Miami University College of Arts and Science and Physics Department startup funding.

APPENDIX : DERIVATION OF $\mathcal{H}_W^{(nl)}$

The derivation of the free waveguide Hamiltonian for the nonlinear case begins with the multimode quantum harmonic oscillator model of the waveguide, which, for the right direction, takes the form

$$\sum_k \omega_{k_R} \hat{a}_{k_R}^\dagger \hat{a}_{k_R} = -\frac{J}{\pi} \iiint \hat{c}_R^\dagger(x) \hat{c}_R(x') \times \cos(k_R) e^{ik_R(x-x')} dx dx' dk_R. \quad (\text{A1})$$

Utilizing the Taylor series expansion of the cosine function, i.e., $\cos(k_R) = \sum_{j=0}^{\infty} \frac{(-1)^j k_R^{2j}}{(2j)!}$, the term under the integral reads as

$$\cos(k_R) e^{ik_R(x-x')} = \left[\sum_{j=0}^{\infty} \frac{\partial_x^{2j}}{(2j)!} \right] e^{ik_R(x-x')}. \quad (\text{A2})$$

Similar to the main paper, we set the lattice constant $L = 1$. Taking the expansion of the cosine as defined in the last equation and inserting it into the right-hand side of Eq. (A1), resulting in the following integral:

$$-\frac{J}{\pi} \iiint \hat{c}_R^\dagger(x) \hat{c}_R(x') \left[\sum_{j=0}^{\infty} \frac{\partial_x^{2j}}{(2j)!} \right] e^{ik_R(x-x')} dx dx' dk_R, \quad (\text{A3})$$

where integrating over k_R and x' and going through a similar calculation for the left direction will then result in the $\mathcal{H}_W^{(nl)}$ as expressed in Eq. (11).

[1] K.-J. Boller, A. Imamoglu, and S. E. Harris, Observation of electromagnetically induced transparency, *Phys. Rev. Lett.* **66**, 2593 (1991).

[2] M. Fleischhauer, A. Imamoglu, and J. P. Marangos, Electromagnetically induced transparency: Optics in coherent media, *Rev. Mod. Phys.* **77**, 633 (2005).

- [3] O. Kocharovskaya, Y. Rostovtsev, and M. O. Scully, Stopping light via hot atoms, *Phys. Rev. Lett.* **86**, 628 (2001).
- [4] A. H. Safavi-Naeini, T. P. M. Alegre, J. Chan, M. Eichenfield, M. Winger, Q. Lin, J. T. Hill, D. E. Chang, and O. Painter, Electromagnetically induced transparency and slow light with optomechanics, *Nature (London)* **472**, 69 (2011).
- [5] R. Walsworth, S. Yelin, and M. Lukin, The story behind “stopped light”, *Opt. Photon. News* **13**, 50 (2002).
- [6] A. I. Lvovsky, B. C. Sanders, and W. Tittel, Optical quantum memory, *Nat. Photon.* **3**, 706 (2009).
- [7] R. G. Beausoleil, W. J. Munro, D. A. Rodrigues, and T. P. Spiller, Applications of electromagnetically induced transparency to quantum information processing, *J. Mod. Opt.* **51**, 2441 (2004).
- [8] J. Kitching, Chip-scale atomic devices, *Appl. Phys. Rev.* **5**, 031302 (2018).
- [9] J. Vanier, Atomic clocks based on coherent population trapping: A review, *Appl. Phys. B* **81**, 421 (2005).
- [10] A. S. Sheremet, M. I. Petrov, I. V. Iorsh, A. V. Poshakinskiy, and A. N. Poddubny, Waveguide quantum electrodynamics: Collective radiance and photon-photon correlations, *Rev. Mod. Phys.* **95**, 015002 (2023).
- [11] D. Roy, C. M. Wilson, and O. Firstenberg, *Colloquium*: Strongly interacting photons in one-dimensional continuum, *Rev. Mod. Phys.* **89**, 021001 (2017).
- [12] Z.-L. Xiang, S. Ashhab, J. Q. You, and F. Nori, Hybrid quantum circuits: Superconducting circuits interacting with other quantum systems, *Rev. Mod. Phys.* **85**, 623 (2013).
- [13] J.-T. Shen and S. Fan, Coherent photon transport from spontaneous emission in one-dimensional waveguides, *Opt. Lett.* **30**, 2001 (2005).
- [14] I. M. Mirza and J. C. Schotland, Influence of disorder on electromagnetically induced transparency in chiral waveguide quantum electrodynamics, *J. Opt. Soc. Am. B* **35**, 1149 (2018).
- [15] Y.-L. L. Fang and H. U. Baranger, Photon correlations generated by inelastic scattering in a one-dimensional waveguide coupled to three-level systems, *Physica E* **78**, 92 (2016).
- [16] P. Bermel, A. Rodriguez, S. G. Johnson, J. D. Joannopoulos, and M. Soljačić, Single-photon all-optical switching using waveguide-cavity quantum electrodynamics, *Phys. Rev. A* **74**, 043818 (2006).
- [17] C. Martens, P. Longo, and K. Busch, Photon transport in one-dimensional systems coupled to three-level quantum impurities, *New J. Phys.* **15**, 083019 (2013).
- [18] Z. R. Gong, H. Ian, L. Zhou, and C. P. Sun, Controlling quasibound states in a one-dimensional continuum through an electromagnetically-induced-transparency mechanism, *Phys. Rev. A* **78**, 053806 (2008).
- [19] L. Zhou, Z. R. Gong, Y.-X. Liu, C. P. Sun, F. Nori *et al.*, Controllable scattering of a single photon inside a one-dimensional resonator waveguide, *Phys. Rev. Lett.* **101**, 100501 (2008).
- [20] M. P. Schneider, T. Sproll, C. Stawiarski, P. Schmitteckert, and K. Busch, Green’s-function formalism for waveguide QED applications, *Phys. Rev. A* **93**, 013828 (2016).
- [21] J. F. M. Werra, P. Longo, and K. Busch, Spectra of coherent resonant light pulses interacting with a two-level atom in a waveguide, *Phys. Rev. A* **87**, 063821 (2013).
- [22] X. Zang and C. Jiang, Single-photon transport properties in a one-dimensional resonator waveguide coupled to a whispering-gallery resonator, *J. Phys. B: At. Mol. Opt. Phys.* **43**, 215501 (2010).
- [23] D. Roy, Correlated few-photon transport in one-dimensional waveguides: Linear and nonlinear dispersions, *Phys. Rev. A* **83**, 043823 (2011).
- [24] M. Hafezi, D. E. Chang, V. Gritsev, E. Demler, and M. D. Lukin, Quantum transport of strongly interacting photons in a one-dimensional nonlinear waveguide, *Phys. Rev. A* **85**, 013822 (2012).
- [25] O. Firstenberg, T. Peyronel, Q.-Y. Liang, A. V. Gorshkov, M. D. Lukin, and V. Vuletić, Attractive photons in a quantum nonlinear medium, *Nature (London)* **502**, 71 (2013).
- [26] N. Fayard, L. Henriët, A. Asenjo-García, and D. E. Chang, Many-body localization in waveguide quantum electrodynamics, *Phys. Rev. Res.* **3**, 033233 (2021).
- [27] A. V. Poshakinskiy and A. N. Poddubny, Dimerization of many-body subradiant states in waveguide quantum electrodynamics, *Phys. Rev. Lett.* **127**, 173601 (2021).
- [28] I. M. Mirza, J. G. Hoskins, and J. C. Schotland, Chirality, band structure, and localization in waveguide quantum electrodynamics, *Phys. Rev. A* **96**, 053804 (2017).
- [29] P. Markos and C. M. Soukoulis, *Wave Propagation: From Electrons to Photonic Crystals and Left-Handed Materials* (Princeton University Press, Princeton, NJ, 2008).
- [30] A. Mostafazadeh, Transfer matrix in scattering theory: A survey of basic properties and recent developments, [arXiv:2009.10507](https://arxiv.org/abs/2009.10507).
- [31] H. J. Kimble, The quantum internet, *Nature (London)* **453**, 1023 (2008).
- [32] D. Witthaut and A. S. Sørensen, Photon scattering by a three-level emitter in a one-dimensional waveguide, *New J. Phys.* **12**, 043052 (2010).
- [33] S. Sen, T. K. Dey, M. R. Nath, and G. Gangopadhyay, Comparison of electromagnetically induced transparency in lambda, cascade and vee three-level systems, *J. Mod. Opt.* **62**, 166 (2015).
- [34] J.-T. Shen and S. Fan, Theory of single-photon transport in a single-mode waveguide. I. Coupling to a cavity containing a two-level atom, *Phys. Rev. A* **79**, 023837 (2009).
- [35] J.-T. Shen and S. Fan, Theory of single-photon transport in a single-mode waveguide. II. Coupling to a whispering-gallery resonator containing a two-level atom, *Phys. Rev. A* **79**, 023838 (2009).
- [36] J. Talukdar and D. Blume, Two emitters coupled to a bath with Kerr-like nonlinearity: Exponential decay, fractional populations, and Rabi oscillations, *Phys. Rev. A* **105**, 063501 (2022).
- [37] M. P. Schneider, A theoretical framework for waveguide quantum electrodynamics and its application in disordered systems, Ph.D. thesis, Humboldt-Universität zu Berlin, Mathematisch-Naturwissenschaftliche Fakultät, 2016.
- [38] A. Carmele, N. Nemet, V. Canela, and S. Parkins, Pronounced non-Markovian features in multiply excited, multiple emitter waveguide QED: Retardation induced anomalous population trapping, *Phys. Rev. Res.* **2**, 013238 (2020).

- [39] P. Yeh, A. Yariv, and C.-S. Hong, Electromagnetic propagation in periodic stratified media. I. General theory, *J. Opt. Soc. Am.* **67**, 423 (1977).
- [40] Z. Liao, H. Nha, and M. S. Zubairy, Single-photon frequency-comb generation in a one-dimensional waveguide coupled to two atomic arrays, *Phys. Rev. A* **93**, 033851 (2016).
- [41] J.-T. Shen, M. L. Povinelli, S. Sandhu, and S. Fan, Stopping single photons in one-dimensional circuit quantum electrodynamics systems, *Phys. Rev. B* **75**, 035320 (2007).